THE ASTROPHYSICAL JOURNAL, 349:625–633, 1990 February 1

RELATIVE ABUNDANCES OF SECONDARY AND PRIMARY COSMIC RAYS AT HIGH ENERGIES

SIMON P. SWORDY, DIETRICH MÜLLER, PETER MEYER, JACQUES L'HEUREUX, AND JOHN M. GRUNSFELD
Enrico Fermi Institute and Department of Physics, University of Chicago
Received 1989 March 2; accepted 1989 July 21

ABSTRACT

We describe new results on the energy spectra of the cosmic-ray nuclei boron, carbon, nitrogen, and oxygen up to energies around 1 TeV per amu. The measurements were performed on the Spacelab 2 mission of the Space Shuttle in 1985. Carbon and oxygen are essentially primary cosmic rays, while boron is purely secondary, and nitrogen has secondary as well as primary contributions. Therefore, the relative abundances of these nuclei provide sensitive information on the propagation of cosmic rays through the Galaxy. We find that the flux of the secondary cosmic rays continues to decrease relative to that of the primaries over the energy range covered with this observation, and that the mean escape length near 1 TeV per amu is about 1 g cm^{-2}.

Subject headings: cosmic rays: abundances — particle acceleration

I. INTRODUCTION

The composition and energy spectra of cosmic-ray nuclei were first studied in the 1960s, leading to a determination of the abundances of the elements up to nickel over a limited range of energies. Two groups of elements were recognized: those nuclei that predominantly originate in the cosmic-ray sources (the primary nuclei), and those species that are produced by spallation in the interstellar medium (the secondary nuclei). Some nuclear species have contributions of both groups in comparable amounts. The initial measurements at low energies, showed that primaries and secondaries have similar energy spectra. It came as a surprise when it was found that at higher energy, above a few GeV per amu, the secondary-to-primary abundance ratio steadily declines (Juliusson, Meyer, and Müller 1972; Smith *et al.* 1973). This energy dependence has since been confirmed in a number of measurements and is known to extend to about 100 GeV per amu (Caldwell 1977; Lezniak and Webber 1978; Simon *et al.* 1980). As the spallation cross sections do not vary significantly at these energies, the energy dependence must be caused by the nature of the cosmic-ray propagation, or, in other words, by the structure of the interstellar medium in the Galaxy.

The observations show that, within measurement errors, the abundance ratio of a pure secondary nucleus to its primary progenitor (e.g., B/C) can be described by a power law in energy or rigidity $R^{-\delta}$ with $\delta = 0.5 \pm 0.1$ at rigidities above 5 GV (for a compilation of various measurements, see Dwyer and Meyer 1987). Within the homogeneous "leaky box" model, where particles escape from the Galaxy with a probability parameterized by an escape path length λ_e, the data imply a power-law dependence $\lambda_e \propto R^{-\delta}$. The path length λ_e represents the mean column density of matter that a particle traverses between the source and the place of escape, or, equivalently, the location of the observer.

Several models have been proposed to describe and understand the energy dependence of the escape mean free path, or, the containment time.

1. Based on earlier work of Kurlsrud and Cesarsky (1971), Audouze and Cesarsky (1973) considered the effect of self-generated waves due to the streaming instability of cosmic rays propagating along Galactic lines of force. This leads to an energy dependence of the longitudinal diffusion coefficient, and therefore a continuous decrease of λ_e with energy.

2. The second model, proposed by Cowsik and Wilson (1973) and further elaborated by Cowsik and Gaisser (1981), Cesarsky and Montmerle (1981), and others, places some cosmic-ray sources into regions of high matter density from which the particles have to escape before propagating in the Galaxy ("nested leaky box"). The escape probability from these source regions is taken to be energy-dependent such that low-energy particles traverse more matter than those of higher energy. At high energy, λ_e would reach a constant level which depends on the residual amount of matter encountered in the interstellar medium.

3. Peters and Westergaard (1977) proposed a model of a very different kind. The assumption is made that the sources of cosmic rays are evenly distributed within the spiral arms of the Galaxy, where the Galactic magnetic field allows a rapid drift of particles along the arms. Outside the spiral arms, within the Galactic disk and halo, cosmic-ray propagation is diffusive, but cosmic rays are retained by large-scale magnetic fields in the halo ("closed Galaxy"). The observational manifestation of this model in the secondary to primary measurements is an initial decrease of the ratio, up to a few hundred GeV per amu, due to less matter being traversed by more energetic (young) particles in the spiral arms. At higher energies the secondary-to-primary ratio will however rise again, as the contributions of old particles from the halo begin to dominate.

Schematically, the energy dependence of the secondary-to-primary abundance ratio (B/C) according to several models is sketched in Figure 1. To distinguish between such models, each of which ascribes very different features to the galaxy, is the challenge for the experiment. The study which we describe in this paper is directed toward this goal.

Most of the previous work on the relative abundances of secondary to primary nuclei at high energies was carried out with balloon-borne instruments (Smith *et al.* 1973; Juliusson 1974; Caldwell 1977; Lezniak and Webber 1978; Simon *et al.* 1980). Exposure times and geometry factors were such that, in view of the steeply falling spectra, statistically significant results could only be obtained up to about 50 GeV per amu. Two detectors were flown on the *HEAO 3* spacecraft: The

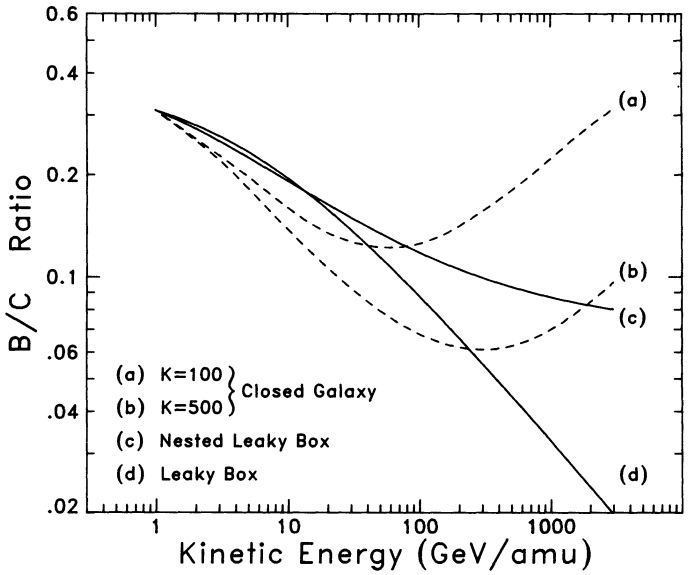

FIG. 1.—The energy dependence of the B/C ratio as predicted by different propagation models: (*a*) The "closed galaxy" model with K, the ratio of the mass in the galaxy to the mass in the spiral arms, as $K = 100$, (*b*) "closed galaxy" model with $K = 500$. (*c*) The "nested leaky box model" with a rigidity-dependent escape $\propto R^{-0.5}$ and residual path length of 1 gm cm^{-2}. (*d*) The homogeneous "leaky box" model with a rigidity-dependent escape $\propto R^{-0.5}$.

measurement of Engelmann *et al.* (1985) covered particle energies below about 25 GeV per amu, and the measurement of Binns *et al.* (1988) led to data for charges $Z \geq 18$ in the 100 GeV per amu region.

Discrimination between the propagation models requires measurements of the abundance ratios at least up to several TeV per amu. As a step in this direction, we developed a detector that has a large geometric factor and that provides good energy measurements in the TeV per amu region. This instrument was exposed on the Space Shuttle for a duration of 8 days in 1985.

In this paper we present the energy spectra of boron and nitrogen, and of their parent nuclei, carbon and oxygen. Boron is a secondary nucleus produced predominantly from spallation of carbon and oxygen. Nitrogen has contributions both of secondary and of primary origin. At low energies the secondary component dominates. Our results on the energy dependence of the B/C and N/O abundance ratios reach to significantly higher energies than previous measurements and have small statistical errors at 100 GeV per amu and below. They are in good agreement in the region of overlap with earlier measurements. Statistical uncertainties imposed by the limited exposure time during the Shuttle flight determine the upper energy limit of our measurements to about 1 TeV per amu. The dynamic range of our instrument reaches to considerably higher energies, which can only be exploited with a longer exposure.

II. INSTRUMENTATION AND SPACELAB 2 FLIGHT

We have used a counter telescope that was flown on the Spacelab 2 mission of the Space Shuttle *Challenger* in July of 1985. A cross section of the instrument is shown in Figure 2. The system consists of (1) two scintillation counters T1 and T2 which are used as a coincidence trigger, for charge determination, and for up-down discrimination with a time-of-flight

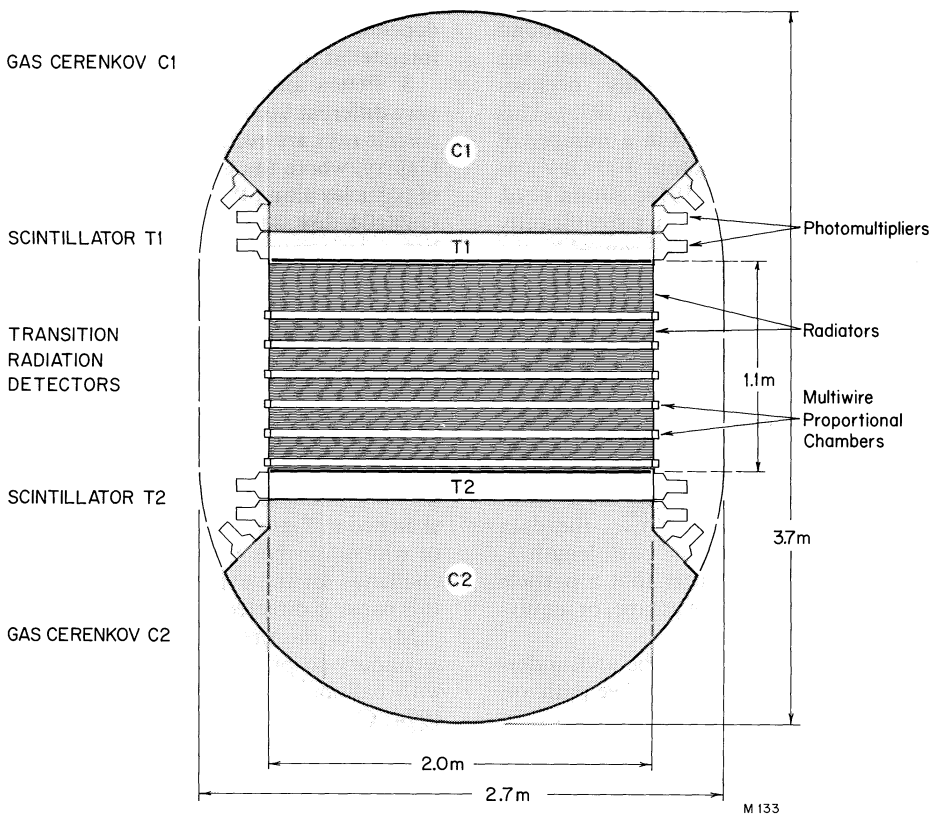

FIG. 2.—Schematic cross section of the instrument

measurement, (2) two integrating gas Cherenkov counters C1 and C2 which provide energy measurements in the 40 to 150 GeV per amu range, (3) a transition radiation detector (TRD) consisting of six layers of radiators and six multi-wire proportional counters (MWPC). The transition radiation intensity determines the particle energy above 500 GeV per amu with good resolution. At lower energies the relativistic increase in the specific ionization in the MWPCs provides a measure of the energy. The MWPCs also serve as a hodoscope for trajectory information. The hodoscope data are used to determine position, zenith angle, and path length of the particle trajectory in each of the detector elements.

The scintillation counters T1 and T2 each consist of a mosaic of nine 1 cm think scintillation segments (NE-110) in a light integration box covered with high reflectance white paint. Each of these counters is viewed by 16 photomultiplier tubes (13 cm diameter windows). From the measurement of the energy loss of the traversing particle, the particle charge is determined after correction for the angle of incidence and for spatial nonuniformities in the light collection efficiency. The same scintillators are also viewed by fast photomultipliers (5 cm diameter windows) to make a time-of-flight measurement between T1 and T2 and thus to determine the direction of incidence of the particles. Charge spectra obtained with just these two counters at energies above 4 GeV per amu and above 90 GeV per amu are shown in Figure 3. The charge resolution (1 σ) at oxygen is 0.2 charge units and does not deteriorate at the higher energy.

The two gas Cherenkov counters C1 and C2 are identical. They and the instrument container are filled with a mixture of 80% N_2 and 20% CO_2 at a pressure of 1 atmosphere. This yields a threshold for Cherenkov light at 40 GeV per amu. The inner walls of the gas Cherenkov counters are coated with high reflectance white paint to efficiently collect the light. The Cherenkov light in each counter is viewed by three groups of 16 PMTs (13 cm diameter UV transparent windows). The threefold division helps to suppress background and provides redundancy in the measurement. The white paint produces a background of Cherenkov light from the passage of the particle through the paint layer. This background corresponds to about 20% to the Cherenkov light signal in saturation, but it exhibits larger fluctuations than expected by photoelectron statistics alone. The contribution of scintillation light in the gas has experimentally been found to be negligible (Lamport *et al.* 1979).

Transition radiation detectors have been used for the first time in this experiment for measurements of the energy of cosmic-ray nuclei. They consist of six layers of radiator interspersed with six multiwire proportional chambers. The radiators are quilts of polyolefin fibers, combining fibers of 4.5 μm and 21 μm diameter. The multiwire proportional chambers are 2 cm thick and covered by thin Mylar lids. The wire spacing is 1 cm but wire groups are joined in 5 cm wide strips which provide sufficient spatial resolution. The pulse heights for each wire group are measured with 12 bit resolution. The chambers are filled with a mixture of Xe, He, and CH_4 (ratio of 25:60:15) at a total pressure of 1 atmosphere. A low flow of this gas is maintained in the multiwire proportional chambers, and a highly sensitive differential pressure gauge keeps the pressure difference δp between the instrument shell and the multiwire chambers to a level $\delta p/p \leq 10^{-5}$. The calibration and detailed behavior of the transition radiation detectors will be the subject of a separate paper (Swordy *et al.* in preparation). The

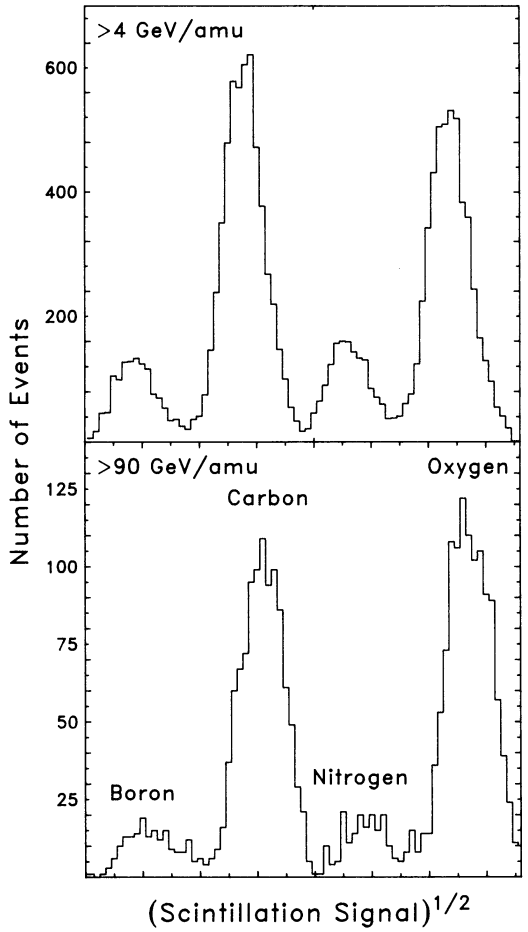

FIG. 3.—The charge spectrum from boron to oxygen obtained from the scintillation counter signals for energies $E > 4$ GeV per amu, and $E > 90$ GeV per amu. Note that the charge resolution does not depend on energy.

MWPCs provide energy measurements in two ways. Up to 500 GeV per amu one observes the relativistic rise which determines the energy with moderate precision. Above 500 GeV per amu the transition radiation X-ray energy added to the ionization energy loss results in a rapid rise in the energy deposited in the chambers. This behavior is shown in Figure 4 which was obtained from accelerator calibrations with singly charged particles. The different techniques used in this instrument lead to variations of the energy resolution with charge and with energy.

Spacelab 2 was launched on 1985 July 29, and returned on 1985 August 6. Its orbit covered a range of latitudes up to 49°.5. Due to different demands on attitude by the various experiments carried on the spacecraft and due to encounters with radiation belt particles at high latitudes and in the South Atlantic anomaly, the effective exposure time was only 78 hours, thereby limiting the statistical accuracy of the measurement.

III. DATA ANALYSIS

The initial analysis procedure (1) selected legitimate events from a total of 4×10^7 event triggers recorded during the flight, (2) corrected the detector pulse heights for spatial and temporal gain variations, and (3) applied several selection criteria to remove background events caused by interactions within the instrument. Subsequent analysis determined the

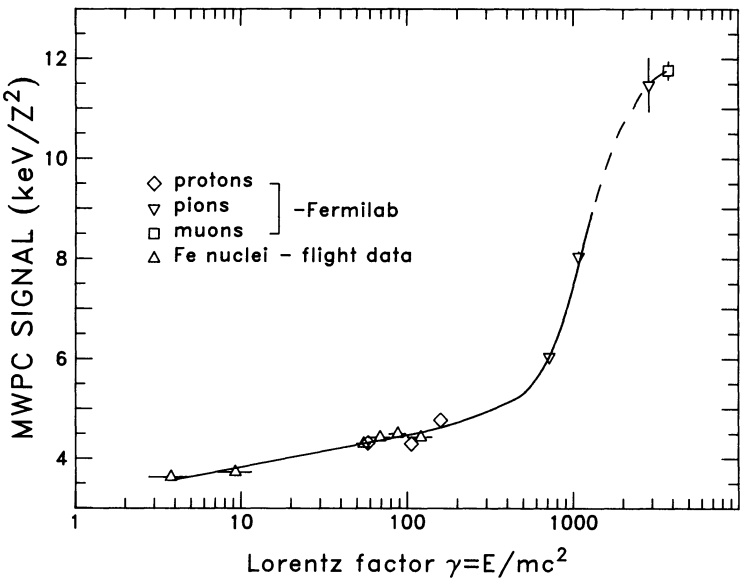

FIG. 4.—The transition radiation detector signal as a function of Lorentz factor γ measured with singly charged particles at Fermilab, except for the open triangles which are for iron nuclei observed in flight.

charge and energy of each event. Corrections for the energy response, efficiency, and interaction corrections were applied to the data from which the energy spectra and flux ratios were derived. These steps are described in more detail in the following.

a) Data Selection and Pulse Height Corrections

The first step in the data analysis was to determine the trajectory of each particle through the instrument. Events were rejected that did not exhibit a clean unambiguous trajectory or that did not show the time of flight signal of a downward moving particle. Events were also rejected if they had trajectories coming from below the Earth's horizon, or coming from directions where the field of view was obstructed by parts of the orbiter or other payloads. All data taken while the orbiter passed through the South Atlantic Anomaly or the horns of the radiation belt were removed from the data set.

The signals from the scintillation counters and the MWPCs were normalized to a vertical path length through the detectors by multiplying the pulse height with the cosine of the zenith angle of incidence. In addition, correction factors were applied to account for spatial nonuniformities. In general, these nonuniformities were less than 5% for the MWPCs, and $\sim 12\%$ (rms) for the scintillators, and were accurately known from calibrations. Small correction factors, on the order of 2% or less, were also applied in order to account for gain drifts due to temperature variations during the flight.

Events were rejected from the data set if the pulse heights implied that an interaction had occurred in the instrument. This includes nuclear interactions and events in which an energetic knock-on electron might have traversed a PMT window. The latter would generate an excessive pulse height in one tube, leading to inconsistent signals between the two independent groups of PMTs in each of the scintillation counters, or between the three independent groups in the Cherenkov counters. The most effective rejection of particles that have undergone spallation in the instrument is the requirement that the signals in the T1 counter and T2 counter agree within $\pm 2\,\sigma$ of the expected pulse height for an individual charge.

The response functions of all counters used in this experiment are well known from preflight calibrations. In particular, we have performed measurements using the Bevalac heavy-particle accelerator to study the response of multiwire proportional chambers to relativistic heavy nuclei and have found that the Z^2 dependence of the signal is strictly valid as long as the total anode signal is below about 10^{-12} coulomb. Therefore, the MWPCs were operated at a gas amplification of ~ 20. We also found that the MWPC pulse height distributions for heavy nuclei become nearly Gaussian, albeit somewhat wider than expected from simple scaling of the response to muons. Details of these calibrations are given by Lamport *et al.* (1979) and Swordy *et al.* (in preparation). The energy dependence of the MWPC signal exhibits the well-known logarithmic increase until, above 500 GeV per amu, transition radiation produces a much sharper rise. This characteristic response has been calibrated with singly charged particles, using beams at Fermilab and at the Bonn electron synchrotron (Swordy *et al.* 1982). Using a bootstrap technique described below, we have verified the expected detector response with flight data. As an example, the response of the MWPCs to iron nuclei in flight is shown in Figure 4. In this case, the energies have been derived from either the Cherenkov signals, or from the geomagnetic cut-off rigidity (see § III*e*). With this technique we also obtained information on statistical fluctuations of signals due to extremely relativistic nuclei that could not be determined with accelerators on the ground.

b) Charge and Energy Assignment

A particle of charge Z and energy E passing through the instrument produces a set of pulse heights x_i in the scintillation counters, in the gas Cherenkov counters, and in the transition radiation counters. To simultaneously analyze the signals we have used a maximum likelihood technique. The likelihood is defined by

$$L(Z, E) = \prod_{i=1}^{n} p_i(x_i; Z, E)\,, \qquad (1)$$

where $p_i(x_i; Z, E)$ is the known probability for a given charge

Z, with energy E to produce a pulse height x_i. We vary Z and E for each event. The values Z, E which maximize the likelihood function are then accepted to characterize this event. The probable error in these parameters is determined from the width of the likelihood distributions.

The form of the probability distributions for each of the three types of counters used in the likelihood analysis was verified using the flight data themselves in the following way: Restrictions were placed on the signals in all the counters except the one of interest, so as to select a particular energy range and charge. For example, the distribution of Cherenkov signals in C1 for a given energy was obtained by selecting events with a specific range of signals in C2, the MWPCs, and the scintillation counters. Permutations of this procedure resulted in a catalog of distributions as a function of charge and energy.

This analysis assigned to each event values for energy and charge, and an estimate of the uncertainty in both quantities.

c) *Energy Deconvolution*

To determine the spectra, the data were sorted according to their energy with intervals chosen to be commensurate with the energy resolution. The quantity $N_m(\Delta E_i)$ is the number of events measured in an energy interval ΔE_i. It would be a direct measure for the particle flux in ΔE_i if the energy resolution of the instrument were perfect. However, due to the finite resolution an overlap correction must be made.

This correction relates the measured number of events $N_m(\Delta E)$ to the corrected value N in the interval ΔE. The number $N(\Delta E)$ represents the differential spectrum dI/dE as $N(\Delta E) \propto \int_{\Delta E} (dI/dE)dE$. The correction is performed according to the matrix relation

$$[N] = [A][N_m]$$

where $[N]$ and $[N_m]$ are column matrices with elements giving the number of events in each energy bin, and $[A]$ is the overlap matrix which must be experimentally determined.

If an accelerator for high-energy nuclei with energies in the range of interest were available, the matrix could be determined directly. Instead, we used a Monte Carlo technique to generate events with energies distributed according to a power law in energy and with signals derived from the known response of the instrument. These simulated events were analyzed with a technique identical to that applied to the real data. This computation determined the connection between the input energy and measured energy for these simulated events and allowed the matrix elements of the overlap matrix to be calculated. The deconvolution correction depends on the assumed spectral index. One therefore must choose an input spectral index that is close to the actual spectral index. A discrepancy between the assumed and the observed spectral index less than 0.1 was found to produce no significant bias.

d) *Geometric and Interaction Corrections, and Selection Efficiencies*

The conversion of the number of events, after applying the deconvolution correction just described, into differential flux values requires knowledge of the geometric factors and exposure times, as well as knowledge of a number of efficiency factors in the data selection, and an estimate of the probability of losses due to nuclear interactions in the instrument. Especially important are possible dependences on charge or energy of these correction factors. To determine the geometric effects and to take into account the mass distribution within the instrument, we have performed a detailed Monte Carlo simulation of particle trajectories through the detector, and to estimate nuclear interaction losses we have assumed that the cross sections are nearly independent on energy in the range of concern here (Bradt and Peters 1950; Westfall *et al.* 1979).

We summarize the various correction factors as follows. (1) *Geometric factor G:* Because of the limited light yield for the Cherenkov counter, for the lower charges ($Z \leq 6$) we have accepted only particles with a relatively long path length in C1 and C2, corresponding to $G = 0.29$ m^2 sr, while a less restricted data set was accepted for heavier nuclei ($Z > 6$), leading to $G = 0.93$ m^2 sr. (2) *Exposure time:* The *effective* exposure time was 3.25 days and the relative instrument deadtime was 28% (in addition, a 12% data loss occurred due to an electronic malfunction). (3) *Interaction losses:* 55% of the carbon nuclei, and 45% of oxygen, are lost due to interaction in the detector, at all energies.[1] (4) *Selection efficiencies:* Efficiencies due to various cuts on the data have been found to vary between 40% and 60% over the range of energies and charges of interest. (5) *Track selection efficiency:* The efficiency with which the hodoscope recognizes clean particle trajectories is about 90%, but is difficult to determine absolutely. Therefore, we have normalized our results relative to oxygen, and the absolute intensity of our oxygen spectrum discussed in the following section, is arbitrarily adjusted to agree with the average of previous oxygen data at 70 GeV per amu, i.e., $(dN/dE)_{\text{oxygen}} = 2.02 \times 10^{-4}$ (m^2 sr s GeV per amu)$^{-1}$.

e) *Low-Energy Data*

Below the Cherenkov threshold, information on the *integral* spectra can be obtained using the Earth's field as a spectrometer. Assuming that the field is produced by a tilted magnetic dipole (of strength 7.92×10^{25} ergs per gauss) located at the center of the Earth we have calculated, for each particle recorded by the instrument, the Störmer rigidity cutoff for the direction of incidence and the position of the spacecraft (Störmer 1955). This model does not include penumbral effects, but we found that the vertical cutoffs predicted by this method are in general agreement with those obtained with a detailed calculation by Shea, Smart, and Carmichael (1976). With this information, we have determined the relative integral fluxes of particles above three rigidity thresholds from 5 to 20 GV. The *differential* flux ratios can be computed from these integral measurements through normalization by a factor which depends on the shape of each energy spectrum, which is rather well known at those low energies. With this technique, we have derived the ratios B/C and N/O at energies below 10 GeV per amu. These values are shown in Figure 6. A systematic error of 10% reflects our estimate of the accuracy of this method. We plan to further refine this analysis in order to deduce the absolute fluxes of the various elemental species at low energies.

IV. RESULTS

This paper addresses the high-energy fluxes and spectra of the four nuclear species boron, carbon, nitrogen, and oxygen, and their relative abundances. The energy spectra measured with our instrument (filled points) as a function of kinetic

[1] This includes interaction losses when particles traverse structural elements inside the detector. The difference between C and O is mainly due to different acceptance criteria [see (1)] leading to a different distribution of particle trajectories.

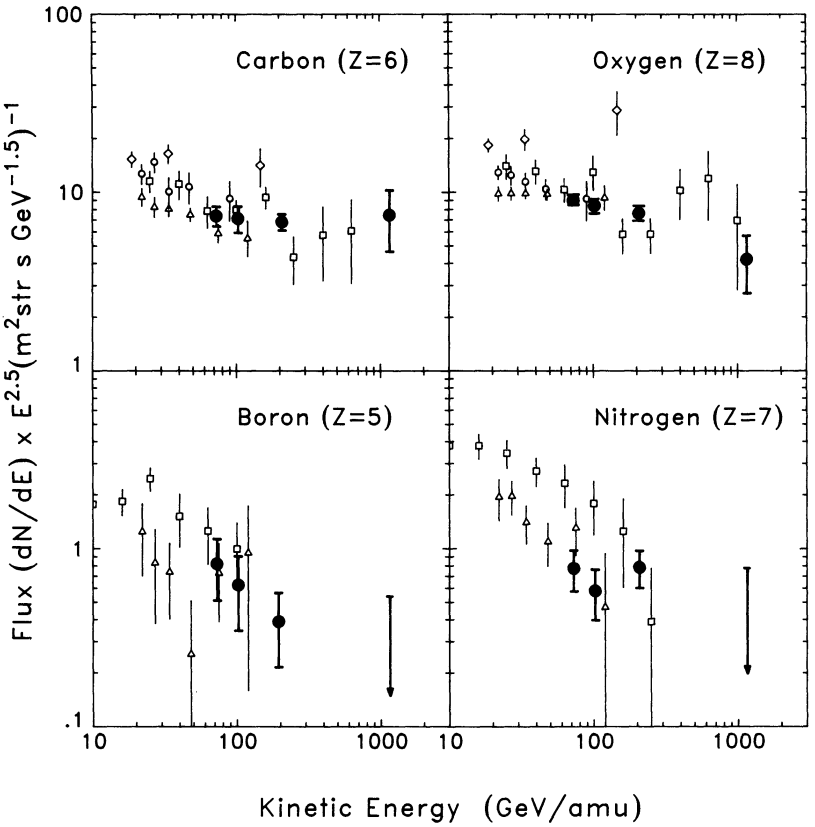

FIG. 5.—Differential kinetic energy spectra for boron, carbon, nitrogen, and oxygen. Note that the flux is multiplied by $E^{2.5}$. *Solid circles:* this experiment; *open circles:* Caldwell 1977; *squares:* Simon *et al.* 1980; *triangles:* Juliusson 1974; *inverted triangles:* Engelmann *et al.* 1985; *diamond:* Orth *et al.* 1978.

energy are shown in Figure 5. The fluxes have been multiplied by $E^{2.5}$, to emphasize spectral differences. The errors are due to counting statistics only since this is the major source of uncertainty. For comparison we include earlier satellite and high-altitude balloon measurements of these fluxes. Table 1 presents the values of our data points, together with the numbers of particles observed in each energy interval. Our flux values are normalized relative to oxygen as discussed above.

The intensity ratios of the secondary to primary nuclei B/C and N/O and that of the primary species C/O are shown in Figure 6 as filled data points. These reflect the variation of secondary to primary nuclei abundance with energy. We should emphasize that the data set accepted for the present analysis is highly restricted in order to eliminate potential systematic errors. Therefore, only a fraction of the events in Figure 3 is retained for the results shown. In a study presently in progress, we are relaxing the acceptance criteria in order to achieve a significant improvement in the statistical quality of the results.

Our results show that both carbon and oxygen have very similar energy spectra, with spectral indices of 2.60 ± 0.1 and 2.65 ± 0.1, respectively. Consequently, the abundance ratio C/O changes little within the experimental uncertainties up to energies in the TeV per amu region. This behavior is expected if both carbon and oxygen are essentially primary nuclei and are produced in the same sources. The spectra of boron and nitrogen, however, are much steeper, and the abundance ratios B/C and N/O continue to decrease up to energies around one TeV per amu. Apparently, the decreasing trend of these ratios that is well established below 50 GeV per amu, does continue to much higher energies.

V. DISCUSSION

In the range of energies covered by these measurements, the cross sections for spallation are essentially independent of energy. Further, above a few GeV per amu, the effects of solar modulation can be neglected. Consequently, the measured ratios of secondary-to-primary nuclei represent the interstellar

TABLE 1

SUMMARY OF RESULTS

γ RANGE	KINETIC ENERGY (GeV per amu)	ACCEPTED NUMBER OF EVENTS				CORRECTED FLUX × 10^{+5} (m2 × str × GeV per amu)$^{-1}$			
		B	C	N	O	Boron	Carbon	Nitrogen	Oxygen
70–90	73	7	61	15	213	1.8 ± 0.7	16.4 ± 2.1	1.74 ± 0.21	20.2 ± 1.4
90–150	103	5	37	10	143	0.59 ± 0.26	6.7 ± 1.1	0.55 ± 0.11	7.9 ± 0.7
150–800	207	5	93	18	209	0.064 ± 0.028	1.1 ± 0.1	0.13 ± 0.03	1.24 ± 0.09
800–10,000	1156	0	7	0	8	0.00064 upper limit	0.017 ± 0.006	0.0017 upper limit	0.0093 ± 0.0033

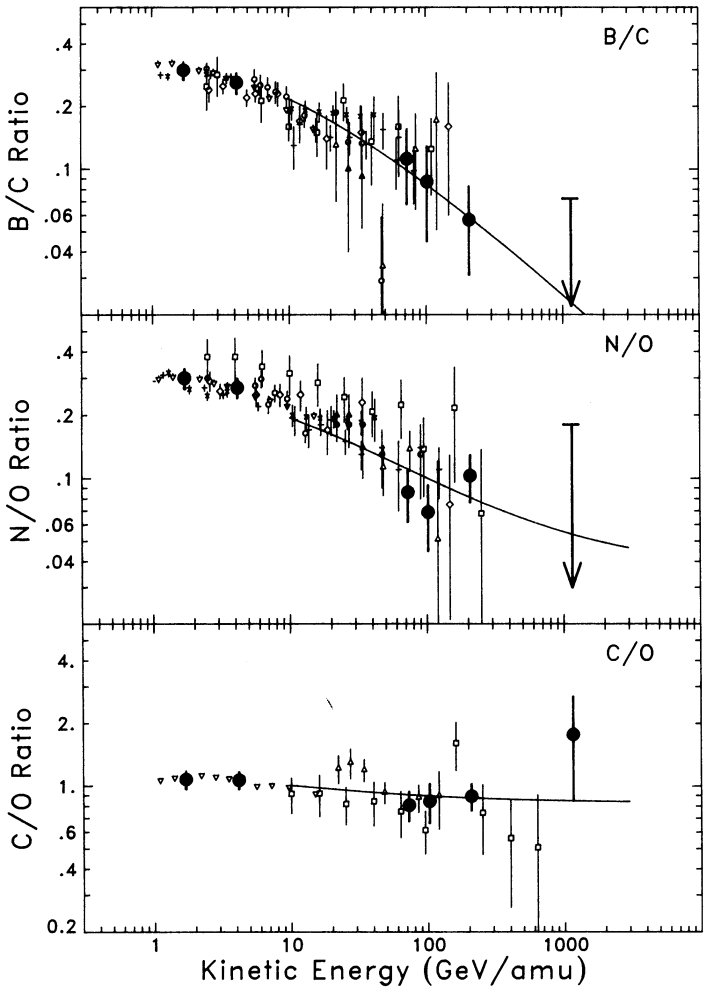

FIG. 6.—The secondary to primary abundance ratios B/C and N/O and the primary to primary abundance ratio C/O as a function of kinetic energy. Symbols are the same as in Fig. 5, and in addition, ×-crosses refer to Lezniak and Webber (1978) and +-crosses to Chappell and Webber (1981). The lines are from a calculation based on the homogeneous leaky box model, with an escape path length proportional to $R^{-0.6}$. The model assumes zero source abundance for boron, but a nitrogen contribution at the source of 4% relative to oxygen.

values and directly reflect the mean path length of material traversed during the propagation of the particles.

As discussed in the Introduction, the energy dependence of the mean path length of the particles in the interstellar material, and hence the energy dependence of the observed secondary to primary ratio, is different for different models of propagation in the Galaxy (see Fig. 1). The "leaky box" model assumes that cosmic rays propagate through the Galaxy without acceleration en route, but have an escape probability, characterized by the mean escape path length λ_e that may depend on energy. As the confinement of cosmic rays is due to the interstellar magnetic fields, it seems natural to express λ_e in terms of rigidity R, and a power-law behavior $\lambda_e \propto R^{-\delta}$ is consistent with many previous measurements. Due to this energy dependence, the propagation path length at high energies will become shorter than the path length against nuclear interaction. The shape of the energy spectrum should then solely be determined by the balance between generation at the source and escape from the Galaxy. Current theories of cosmic-ray acceleration via interstellar shocks (Völk 1987; Axford 1981) predict that the *source spectrum* of cosmic rays be a power law in momentum of rigidity of the form $dS/dE \propto R^{-(2+\epsilon)}$, where ϵ is a parameter related to the strength of the shock. The energy-dependent leaky box model then predicts for the *observed spectrum* at high energies (i.e., when spallation can be ignored) the form $dI/dE \propto R^{-(2+\epsilon+\delta)}$ for primary nuclei, and $dI/dE \propto R^{-(2+\epsilon+2\delta)}$ for secondaries.

In order to accurately determine the energy dependence of λ_e from the secondary/primary ratio, we must assume that the secondary nucleus has a negligible source abundance at all energies. Boron is believed to be such a nucleus.

We therefore compute the B/C ratio at high energies in the context of a "leaky box" model of the Galaxy. This model implicitly assumes an exponential distribution of propagation path lengths. In the energy region above 10 GeV per amu, we can greatly simplify the model calculation since the effects of energy loss during propagation and of solar modulation are small enough to be neglected. We use the semiempirical values of Tsao and Silberberg (1979) for the cross sections for spallation into lighter nuclei, and we assume the relative abundances of the primary nuclei C, O, Ne, Mg, Si, and Fe, to be given by Hinshaw and Wiedenbeck (1983). As shown in Figure 6 the following parameterization is a good fit to both our results and the data of others:

$$\lambda_e(R) = 6.9\left(\frac{R}{20\ \mathrm{GV}}\right)^{-0.6}\ \mathrm{g\ cm^2} \quad (R > 20\ \mathrm{GV})\ .$$

It should be noted that a range of values for δ between

approximately 0.5 and 0.7 would give comparably good fits to our data. The value given above is further constrained by the data of other workers at ≈ 10 GeV per amu.

This situation with nitrogen is different as this element, while mostly secondary in origin, does have a small primary contribution. A recent analysis of the abundance of nitrogen isotopes (Krombel and Wiedenbeck 1988) indicates that the relative abundance of $^{14}N/^{16}O$ in the source is 0.037 ± 0.017. It is generally believed that no ^{15}N is generated in the source. Thus we show, in Figure 6 our data on the N/O ratio together with the results of a leaky box calculation using the same parameters which provided a good fit to the B/C data shown above, but assuming a 4% contribution of nitrogen nuclei at the source. This calculations fits our measurement of N/O at high energies quite well. However, the trend of our fitted curve, extrapolated to lower energies, seems to undershoot the measured data. This discrepancy can be resolved if recent data on the interaction cross sections at low energy are taken into account (Gupta and Webber 1989).

Our model predicts that the secondary-to-primary ratio decreases continually with increasing energy. However, in the region above a few hundred GeV per amu the measurements do not exclude the possibility that the ratio becomes constant, consistent with a residual pathlength of $\lambda_e \approx 1$ g cm^{-2}. Thus our data are not in conflict with the "nested" leaky box assumption. Within the experimental uncertainties, the data do not show an indication for an increase of the secondary/primary ratio at high energy as expected for the "closed galaxy" model.

Depending on the propagation model, the interstellar matter could either be concentrated near the source (nested leaky box model), or it could be uniformly distributed (leaky box model), or it could be a mixture of both. If it is uniformly distributed, the path length is proportional to the containment time τ of particles in the Galaxy, and an estimate of this time can be made. Measurements of the proportion of the radioactive isotope ^{10}Be at energies below 1 GeV per amu indicate $\tau \approx 1.5 \times 10^7$ years (Simpson and Garcia-Munoz 1988) and imply a mean material density in the containment volume of ≈ 0.24 atoms cm^{-3}. For the same density of material, in the TeV per amu region the value of $\lambda \approx 1$ g cm^{-2} would suggest a containment time of $\approx 2 \times 10^6$ years. This time can be compared with an estimate of the electron lifetime. The interpretation of the measured electron spectrum (Prince 1979; Nishimura *et al.* 1985; Tang 1984) gives $\tau \approx 10^7$ years in the 10–100 GeV region, but does not provide strong evidence for an energy dependence. This inconsistency has been taken as an argument in favor of a nested leaky box model (Tang and Müller 1983).

An important difference between the energy-dependent leaky box model and the nested leaky box model is the spectral shape of the source spectra. If all species are generated with the same spectra *at the source*, the *observed* primary spectra at high energies would be steepened by the factor $R^{-\delta}$ in the first case. In the second, the source spectrum and the observed spectrum would have the same slope. Thus, the source spectrum would be $\sim R^{-2.2}$ for the homogeneous leaky box but $\sim R^{-2.7}$ for the nested leaky box. The most attractive mechanism for accelerating these particles, that of diffusive shock acceleration, could provide either of these indices, depending on the compression ratio at the shock, (which would be larger for the harder spectrum with $\Gamma = 2.2$).

In summary, the work reported here demonstrates that the escape mean free path λ_e for Galactic cosmic rays continues to decrease with energy, at energies beyond 100 GeV per amu. We observe that near 1 TeV per amu the mean escape length of particles is ≈ 1 g cm^2 as compared to ≈ 9 g cm^2 at 1 GeV per amu. Our results are limited by counting statistics. An exposure of the instrument for a time period of ~ 1 year would be required to extend the measurements by another order of magnitude in energy, and in order to substantially increase the statistical accuracy.

This work would not have been possible without the devoted efforts of the staff of our laboratory, in particular of Mrs. L. Glennie, and Messrs. D. Bonasera, E. Drag, W. Harvey, W. Johnson, and R. Ray. We also acknowledge contributions to the data analysis by A. Borione, M. Kamionkowski, and L. Kawano. Finally, our thanks go to the Spacelab-2 team of the NASA Marshall Space Flight Center and, in particular, to Dr. Roy Lester.

This work was supported by NASA under contract NAS 8-32828 and grants NAG W-1311, NGL 14-001-005, and NGL 14-001-258. J. M. G. Grunsfeld acknowledges support under a W. D. Grainger Postdoctoral Fellowship.

REFERENCES

Audouze, J., and Cesarsky, C. J. 1973, *Nature Phys. Sci.*, **241**, 98.
Axford, W. I. 1981, *Proc. 17th Internat. Cosmic Ray Conf.* (Paris), **12**, 155.
Binns, W. R., Garrard, T. L., Israel, M. H., Jones, M. D., Kamionkowski, M. P., Klarman, J., Stone, E. C., and Waddington, J. C. 1988, *Ap. J.*, **324**, 1106.
Bradt, H. C., and Peters, B. 1950, *Phys. Rev.*, **77**, 54.
Caldwell, J. H. 1977, *Ap. J.*, **218**, 269.
Cesarsky, C. J., and Montmerle, T. M. 1981, *Proc. 17th Internat. Cosmic Ray Conf.* (Paris), **9**, 207.
Chappell, J. H., and Webber, W. R. 1981, *Proc. 17th Internat. Cosmic Ray Conf.* (Paris), **2**, 59.
Cowsik, R., and Gaisser, T. K. 1981, *Proc. 17th Internat. Cosmic Ray Conf.* (Paris), **2**, 218.
Cowsik, R., and Wilson, L. W. 1973, *Proc. 13th Internat. Cosmic Ray Conf.* (Denver), **1**, 500.
Dwyer, R., and Meyer, P. 1987, *Ap. J.*, **322**, 981.
Engelmann, J. J., Goret, P., Juliusson, E., Koch-Miramond, L., Lund, N., Masse, P., Rasmussen, I. L., and Soutoul, A. 1985, *Astr. Ap.*, **148**, 12.
Garcia-Munoz, M., Simpson, J. A., Guzik, T. J., Wefel, J. P., and Margolis, S. H. 1987, *Ap. J. Suppl.*, **64**, 269.
Grunsfeld, J. 1988, Ph.D. thesis, University of Chicago.
Gupta, M., and Webber, W. R. 1989, *Ap. J.*, **340**, 1124.
Hinshaw, G. F., and Wiedenbeck, M. E. 1983, *Proc. 18th Internat. Cosmic Ray Conf.* (Bangalore), **9**, 263.
Juliusson, E. 1974, *Ap. J.*, **191**, 331.
Juliusson, E., Meyer, P., and Müller, D. 1972, *Phys. Rev. Letters*, **29**, 445.
Krombel, K. E., and Wiedenbeck, M. E. 1988, *Ap. J.*, **328**, 940.
Kurlsrud, R. M., and Cesarsky, C. J. 1971, *Ap. Letters*, **8**, 189.
Lamport, J. E., L'Heureux, J., Meyer, P., and Müller, D. 1979, *Proc. 16th. Internat. Cosmic Ray Conf.* (Kyoto), **11**, 62.
Lezniak, J. A., and Webber, W. R. 1978, *Ap. J.*, **223**, 676.
Nishimura, J., *et al.* 1985, *Proc. 19th Internat. Cosmic Ray Conf.* (La Jolla), **9**, 539.
Orth, C. D., Buffington, A., Smoot, G. F., and Mast, T. 1978, *Ap. J.*, **226**, 1147.
Peters, B., and Westergaard, N. J. 1977, *Ap. Space Sci.*, **48**, 21.
Prince, T. A. 1979, *Ap. J.*, **227**, 676.
Shea, M. A., Smart, D. F., and Carmichael, H. 1976, AFGL-TR-76-0015, Air Force Geophysical Laboratory, Hanscom AFB, Mass.
Simon, M., Spiegelhauer, H. Schmidt, W. K. H., Siohan, F., Ormes, J. F., Balasubramanyan, V. K., and Aren, J. F. 1980, *Ap. J.*, **239**, 712.
Simpson, J. A., and Garcia-Munoz, M. 1988, *Space Sci. Reviews*, **46**, 205.
Smith, L. H., Buffington, A., Smoot, G. F., Alvarez, L. W., and Wahlig, M. A. 1973, *Ap. J.*, **180**, 987.

Störmer, C. 1955, *The Polar Aurorae*, New York: Oxford University Press.
Swordy, S. P., L'Heureux, J., Müller, D., and Meyer, P. 1982, *Nucl. Instr. Meth.*, **193**, 591.
Tang, K.-K. 1984, *Ap. J.*, **278**, 881.
Tang, K.-K., and Müller, D. 1983, *Proc. 18th Internat. Cosmic Ray Conf.* (Bangalore), **9**, 251.
Tsao, C. H., and Silberberg, R. 1979, *Proc. 16th Internat. Cosmic Ray Conf.* (Kyoto), **2**, 202.
Völk, H. J. 1987, *Proc. 20th Internat. Cosmic Ray Conf.* (Moscow), **7**, 157.
Westfall, J. D., Wilson, L. W., Lindstrom, P. J., Crawford, H. C., Greiner, D. E., and Heckman, H. H. 1979, *Phys. Rev. C*, **19**, 1309.

JOHN M. GRUNSFELD, JACQUES L'HEUREUX, PETER MEYER, DIETRICH MÜLLER, and SIMON SWORDY: University of Chicago, Enrico Fermi Institute, 993 East 56th Street, Chicago IL 60637